PHYSICAL REVIEW B **82**, 144304 (2010)

Exchange interaction function for spin-lattice coupling in bcc iron

Hai Wang, Pui-Wai Ma,* and C. H. Woo†
Department of Electronic and Information Engineering, The Hong Kong Polytechnic University, Hong Kong, SAR, China
(Received 31 May 2010; revised manuscript received 12 August 2010; published 18 October 2010)

Functional representations of the spin polarization and the exchange interaction in terms of the lattice configuration is necessary to model the dynamics of the coupled spin and lattice subsystems in large-scale atomistic simulation of magnetic materials. Data needed for this purpose have only existed in the regime of small displacements from the equilibrium perfect lattice configurations. In this paper, we report and discuss the results of our first-principles calculations for bcc iron over a wide range of lattice constants using the magnetic force theorem and the one-electron Green's function. Despite the relatively complex functional form of the exchange interaction function for bcc iron our results show that it can be expressed as a superposition of Bethe-Slater-type curves representing interatomic exchange interaction of the 3*d* electrons.

DOI: 10.1103/PhysRevB.82.144304 PACS number(s): 75.30.Et, 75.50.Bb

I. INTRODUCTION

Magnetic effect is well known to play a pivotal role in the structural stability of iron.[1] For example, the softening of tetragonal shear modulus $C'=\frac{1}{2}(C_{11}-C_{12})$ at elevated temperature[2–4] and the resulting change in dominant orientation of dislocation loops from ⟨110⟩ to ⟨100⟩ at around 500 °C, are believed to be results of the magnetic effect.[5–7] Using Monte Carlo simulation and magnetic cluster expansion model, Lavrentiev *et al.*[8] also showed that magnetic fluctuations are responsible for the bcc-fcc phase transition of iron at 1184 K, which is slightly higher than the Curie temperature T_C at 1043 K.

Although a*b initio* calculations are powerful tools in the exploration of ground-state properties of materials, it is in general difficult to extend its application to cases where the interactions among many-body elementary excitations are strong. Attempts to use the Fermi distribution to mimic finite-temperature behavior of electrons in materials[9] are restricted to cases where the dynamic interactions among the electrons, the spin waves, and the lattice vibrations are sufficiently weak, which almost certainly excludes the strong-interaction regime near phase transitions.

To enable the investigation of the strongly interactive spin and lattice dynamics at higher temperatures, Antropov *et al.*[10] suggested that the interactions between atoms, including the exchange interaction J_{ij}, can be obtained via *ab initio* calculations. The dynamics of the interactive atoms and the coupled spins, as represented by the Heisenberg Hamiltonian, can then be integrated using classical molecular dynamics and spin dynamics simulations, respectively. Nevertheless, the suggestion remains untested. The computer resources required are expected to be tremendous and even prohibitive in the actual implementation.

By explicitly incorporating a magnetic term in the functional form of the empirical many-body potential, Dudarev and Derlet[11–13] proposed the first magnetic potential for atomistic simulations at 0 K. The magnetic effect due to this potential stabilizes the dumbbell configuration so that the ground-state self-interstitial configuration in bcc iron is not the ⟨111⟩-crowdion but the ⟨110⟩-dumbbell, which is consistent with the *ab initio* calculations.[14,15]

Recently, Ma *et al.*[16,17] developed the spin-lattice dynamics (SLD) simulation scheme in which the coupled spin and lattice degrees of freedom are treated on equal footing in the equations of motion of the system. The dynamics of the coupled systems is then described in terms of the empirical many-body potential among the atoms and the exchange interaction function (EIF) among the spins. The interaction between the spin and lattice waves (magnons and phonons) in SLD is realized through the dependence of the EIF on the atomic configuration in the neighborhood. The importance of the coupling between the spin waves and the lattice vibrations (i.e., the spin-phonon interaction) to the mechanical properties of bcc iron thin film has been demonstrated.[16,17]

Within the tight-binding representation, the intersite contribution to the total exchange energy of the crystal can be expressed to a good approximation as a sum of two-center integrals involving nearest-neighbor (NN) pairs.[18] This suggests that the exchange interactions are mainly two-body interactions, at least between nearest-neighbor pairs, and the EIF between atoms i and j may be represented as a function of the interatomic distance. Indeed, using the EIF fitted accordingly has yielded good results for near-equilibrium perfect crystal properties.[16] Nevertheless, a more extensive database for the EIF is needed for more complex configurations in applications such as dislocations, interstitial clusters, high-energy displacement cascades, etc. The present work is an effort toward this goal. In this regard, information on the EIF for short interatomic distance is particularly lacking.[19,20] At the same time, the importance of contributions from many-body effects, particularly when second and higher nearest neighbors are involved also has to be clarified.

In addition, the dependence of the magnitude of the atomic spin on the atomic environment in Refs. 16 and 17 is subsumed into the EIF for convenience. Physically, the variation in the atomic spin polarization occurs via the atomic volume that governs the space available for the on-site electrons to stay away from each other to facilitate spin alignment by avoiding Pauli's exclusion. The variation of the magnitudes of the spins in a local region is a many-body rather than a two-body effect. It has a different functional dependence from the EIF and should be considered and modeled separately.

In the following, we calculate over a wide range of lattice constants the spin-split density of states (DOS), the electron density maps, the atomic magnetic moments (MMs), and the exchange interaction parameter between different neighbors of bcc iron. The relation between the functional behavior and the electronic structure is then considered via the spin-split DOS and the electron-density maps. The utility of the data obtained as a base to formulate the EIF as a function of interatomic distance and neighboring atomic configuration is discussed.

II. METHODOLOGY

The magnetic energy due to exchange interaction among atoms can be expressed by the Heisenberg Hamiltonian in the form[21,22]

$$H = -\sum_{i \neq j} J_{ij} \mathbf{S}_i \cdot \mathbf{S}_j, \tag{1}$$

where J_{ij} is the exchange interaction between atoms i and j, and $\mathbf{S}_i$ is the total spin of atom i. The MM of atom i associated with $\mathbf{S}_i$ has a magnitude $M_i = g\mu_B S_i$, where S_i is the magnitude of the atomic spin and $g=2.0023$ is the electronic g factor. Here, we adopt the convention that the direction of the atomic spin is opposite to the MM. For the perfect crystal, all atoms are equivalent and the subscript i in M and S can be dropped.

If $J_{ij} > 0$, the Heisenberg Hamiltonian in Eq. (1) provides the restoring force to align the spins or MMs of neighboring atoms to stabilize the ferromagnetic phase below the Curie temperature. The exchange interaction depends sensitively on the corresponding interatomic separation between atoms i and j, through the overlap of the atomic orbitals. At the same time, the atomic volume plays a key role in determining the magnitude M of the atomic MMs via the spin polarization of the on-site electrons as functions of the atomic density.[21] For convenience, Eq. (1) is also sometimes written as an effective Hamiltonian in the form[23,24]

$$H = -\sum_{i \neq j} J_{ij}^{eff} \mathbf{e}_i \cdot \mathbf{e}_j, \tag{2}$$

where $\mathbf{e}_i$ is the unit vector of the atomic spin at site i. J_{ij}^{eff} is an effective exchange coupling parameter with the magnitudes of S_i and S_j subsumed into it. For small changes in the atomic separation, S and M can be assumed constant, J_{ij}^{eff} and J_{ij} may be used interchangeably. However, in the present consideration the magnitude of the atomic spins[19,20] may vary substantially over an extended range of atomic densities (separations). As mentioned in Sec. I, these two factors of J_{ij}^{eff} have different physical meanings and functional dependencies, and should be considered and modeled separately.

In the following, we first calculate the spin-polarized electronic structure of bcc iron over a range of lattice constants from 2.2 to 3.2 Å. Two computer codes are employed, WIEN2K (Ref. 25) based on the full-potential linearized augmented plane-wave (FP-LAPW) method, and a private code based on the linear muffin-tin orbital (LMTO) method[23,26–29] within the atomic spheres approximation (ASA). Using the magnetic force theorem[30–32] and the one-electron Green's function (GF), J_{ij}^{eff} is calculated using LMTO-GF.[28,29] A thorough review on EIF and the corresponding analytic derivation can be found in Ref. 23. In brief, the EIF connecting site i and j can be written as

$$J_{ij}^{eff} = \frac{1}{4\pi} \mathrm{Im} \int^{E_F} \mathrm{Tr}_L [\Delta_i g_{ij}^{\uparrow} \Delta_j g_{ji}^{\downarrow}] dE, \tag{3}$$

where Tr_L denotes the trace over angular momentum indices $L=(l,m)$, $g_{iL,jL'}^{\sigma}(z) = \{[P^{\sigma}(z) - S]^{-1}\}_{iL,jL'}$ is the auxiliary Green's-function matrix for a complex energy z, $\Delta_i = P_i^{\uparrow} - P_i^{\downarrow}$ is a on-site perturbation, $P_{iL,jL'}^{\sigma} = P_{iL}^{\sigma} \delta_{iL,jL'}$ is a site-diagonal matrix of potential functions, and S is a potential-independent structure constant.

The total, partial, as well as $3d$-e_g and $3d$-t_{2g} components of the DOS are calculated, together with the MM per atom. While WIEN2K may be superior for electronic-structure calculations, it is not equipped to calculate the exchange interaction. Using the magnetic force theorem[30–32] and the one-electron GF, J_{ij}^{eff} is calculated using LMTO-GF, from which J_{ij} can be calculated from the MM using $J_{ij} = (\frac{g\mu_B}{M})^2 J_{ij}^{eff}$. We note that $\frac{g\mu_B}{M}$ is unitless, so that J_{ij} and J_{ij}^{eff} have the same unit (mRy).

The $Im\bar{3}m$ space group is used to describe the symmetry for bcc iron. Brillouin-zone integrals are calculated using a $40 \times 40 \times 40$ k-points mesh. There are all together 1661 irreducible k points. For the generalized gradient approximation (GGA), the Perdew-Burke-Ernzerhof (PBE) scheme is used.[33] For the local-density approximation (LDA), Perdew and Zunger[34] is used in WIEN2K, and von Barth and Hedin[35] is used in LMTO-GF. Since LDA does not gives the correct ground state of bcc iron,[36] many investigations[37] on the electronic and magnetic properties of bcc iron are performed using GGA that gives the correct ground state.[38] Our results reported in the following are mainly based on GGA. LDA results are presented only for reference.

In the WIEN2K calculations, we set $R_{\mathrm{mt}} K_{\mathrm{max}} = 10$, where R_{mt} is the muffin-tin radius set to maximize the muffin-tin sphere volume and K_{max} is the maximum reciprocal-space vector. We also set the maximum number of the spherical harmonics in the atomic spheres $l_{\mathrm{max}}+1$ to 12, and the largest reciprocal vector in the charge Fourier expansion G_{max} to 15. In LMTO-GF, R_{mt} is set equal to the radius of the Wigner-Seitz cell.

The convergence of J_{ij}^{eff} with respect to the number of k points is assessed with a progressively finer mesh. We use a mesh of $70 \times 70 \times 70$ k points corresponding to 8112 irreducible k points. For a lattice constant of 2.8665 Å, J_{ij}^{eff} converges with an accuracy of $\sim 2\%$ while the total energies converges to within $\sim 0.5\%$, which is the tolerance we set for the present calculations.

III. RESULTS AND DISCUSSIONS

Figure 1 shows the total energy we obtain with WIEN2K and LMTO-GF using GGA-PBE for various lattice constants. The results from WIEN95 (Ref. 1) and the experiments[39] are also plotted for comparison. The consis-

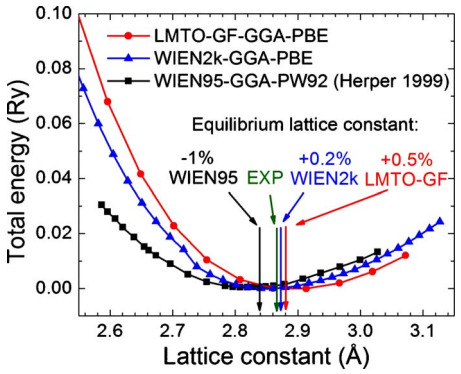

FIG. 1. (Color online) Total energy as a function of lattice constant calculated with different models.

tency among the different methods is very good and well within the tolerance of 0.5% of the calculations. Fitting the energy-volume data to Birch-Murnaghan equation of state,[40] the equilibrium lattice constant, bulk modulus, and pressure are obtained. Equilibrium values of the lattice constant, the corresponding MM, and bulk modulus obtained with WIEN2K are 2.873 Å, 2.25 μ_B, and 1.73 Mbar, respectively. Similar values obtained with LMTO-GF are 2.881 Å, 2.26 μ_B, and 1.79 Mbar. All the values are in excellent agreement with each other and with experimental values of 2.8665 Å,[39] 2.22 μ_B,[41] and 1.72 Mbar.[41] These results are also consistent with other theoretical works.[1,37,42]

Using the same set of data, we calculate and plot in Fig. 2 the MM as a function of the lattice constant. Results obtained following Kormann *et al.*[24] are also shown for comparison. Good consistency can be seen among results from the different methods. Except for small lattice constants, the MM calculated with WIEN2K and LMTO-GF vanish at around 2.3–2.4 Å, showing the loss of stability of the spin-polarized state of the on-site electrons at high atomic density.[19,20] The difference in the two results is mainly due to errors caused by the ASA in the LMTO-GF model, which involves replacing the Wigner-Seitz cell with an atomic sphere of equal volume. The sudden drop of the MM in the case of LMTO-GF could also be due to the same reason. Nevertheless, the overall disagreement of the MM between

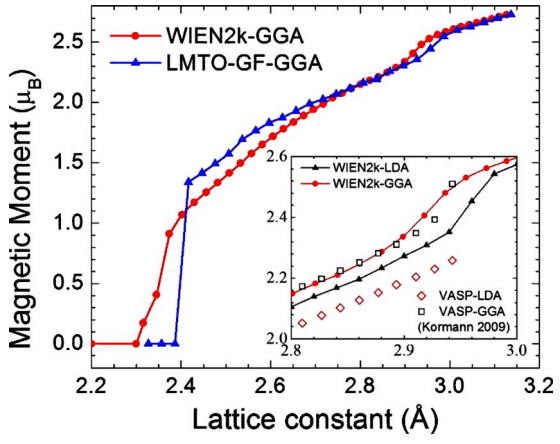

FIG. 2. (Color online) Calculated MM as a function of lattice constant.

the two models is small, showing similar magnetic/nonmagnetic transition at a lattice constant of ~2.3 Å, and the characteristic inflection point near ~2.90 Å. In addition, the present results are consistent with those obtained by Kormann *et al.*[24] using VASP with GGA, which is also shown in the inset of Fig. 2. The characteristic inflection point of the MM also occurs in our LDA calculations, but not in Ref. 24, where it appears at a slightly larger lattice constant. There is no clear explanation of this characteristic inflection point of the MM in the literature. The reduction in the MM with the atomic volume is due to the reduction in the on-site spin polarization caused by the higher atomic density. This limits the available space for the onsite electrons to stay apart from each other to remain aligned by minimizing the effects of Pauli's exclusion. This creates a many-body effect on the spin-spin interaction as expressed by the Heisenberg Hamiltonian in Eq. (1).

The total DOSs for lattice constants 2.25 Å, 2.45 Å, and 2.88 Å calculated using LMTO-GF and WIEN2K are plotted and compared in Figs. 3(a) and 3(b), respectively. Good agreements are found between the two models in all cases. Comparison with existing results for the equilibrium lattice in the literature also shows good consistency.[43,44] In (i) of Figs. 3(a) and 3(b), we show the DOS of the highly compressed nonspin-polarized (nonmagnetic) state (MM=0) of bcc iron. Increasing the atomic volume by increasing the lattice parameter from 2.25 to 2.45 Å restores ferromagnetism by removing the spin degeneracy and splitting the DOS accordingly into majority- and minority-spin components. The results can be seen in (ii). The unfilled majority-spin subband at the calculated equilibrium lattice constant 2.88 Å in (iii) is consistent with the weakly ferromagnetic nature of bcc iron. In these figures, we also note the small *s* and *p* contributions to the total DOS, and the practically complete dominance of the 3*d* contributions. The foregoing results are consistent with the findings of Refs. 45 and 46, where the Coulomb correlation loses importance with increasing atomic density and that ferromagnetic metals such as Fe, Co, and Ni are all presumed nonmagnetic under high pressure.[19,20,47,48]

Bcc iron has O_h symmetry and the 3*d*-DOS is split into the triply degenerate t_{2g} and doubly degenerate e_g components. The partial DOS of the t_{2g} and e_g states are, respectively, shown in Figs. 3(c) and 3(d). The occupancy of each spin subband, obtained by integrating the partial DOS up to the Fermi level, is shown. The t_{2g} bands are ~65% occupied and e_g bands are slightly less (~58%). This is somewhat smaller than the 70% occupancy in the atomic state. As atoms in the highly compressed nonmagnetic state move apart, the Pauli exclusion that favors the antiparallel spin configuration weakens and the Coulomb exchange correlation that favors the parallel spin configuration starts to dominate. Splitting of both the t_{2g} and e_g spin subbands starts to occur beyond 2.3 Å (Fig. 2) as can be seen in (ii) of Figs. 3(c) and 3(d). The splitting becomes very obvious in (iii). Indeed, in this case, there are twice as many electrons with majority than with minority spin in the t_{2g} band. This proportion is even higher (~3.5 times) in the e_g band. The 3*d* majority-spin subband is almost, i.e., 80–90 %, full. The minority-spin subband, on the other hand, are only ~40% occupied and

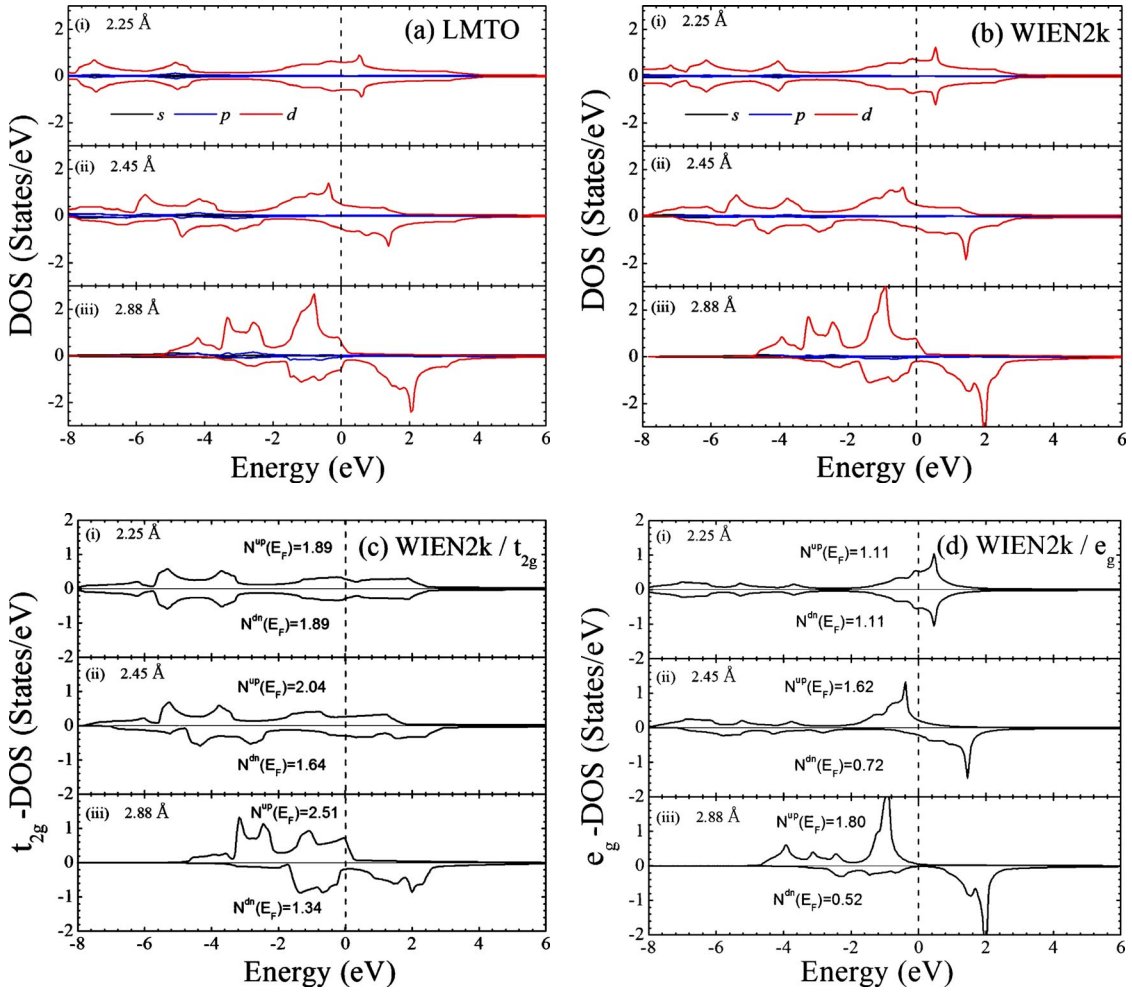

FIG. 3. (Color online) The partial DOS of bcc Fe using (a) LMTO-GF and (b) WIEN2K methods for different lattice constants: (i) 2.25 (ii), 2.45, and (iii) 2.88 Å. The t_{2g} and e_g components of the 3d-DOS are shown in (c) and (d) panels, respectively.

predominantly (~75%) by t_{2g} electrons. This is consistent with the results of Jones *et al.*[49] Unequal occupancy of the spin subbands creates a MM and drives the nonmagnetic/ferromagnetic transition as the lattice parameter increases beyond 2.3 Å.

The 3d-DOS for the near-equilibrium lattice constants, 2.77, 2.88, 2.91 and 2.94 Å, are shown in Fig. 4(a). Contributions from the t_{2g} and e_g bands are also, respectively, presented in Figs. 4(b) and 4(c). In this range, one may notice that changing the lattice parameter has more influence on the bandwidth, energy shift, and the DOS at the Fermi level of the t_{2g} state than the e_g state. This is also reflected in the inflection point of the magnetic moment as a function of the lattice constant seen in Fig. 2, which may be related to the relatively large change in the t_{2g} DOS at the Fermi level.

Figure 5 shows the corresponding electron density maps of bcc Fe on the $(1\bar{1}0)$ plane for the four lattice constants as in Fig. 4. The two columns are for the majority- and minority-spin densities as marked. The x axis is along the ⟨110⟩ third NN direction, the y axis is along the ⟨001⟩ second-NN (2NN) direction, and the diagonal is along the ⟨111⟩ first-NN (1NN) direction. Thus, AB and BC are 1NNs, BC and B′C′ are 2NNs, and BB′ and CC′ are third NNs.

The topological structure of the electron densities for the equilibrium lattice constant (2.88 Å) presented in Fig. 5 is very much in line with those of Jones *et al.*[49] The difference between the electron-density distributions for two spin states is obvious with the minority spins showing stronger bonding tendency than the majority spins. In this regard, the minority spins mostly occupy the t_{2g} states (note the square shape of the electron cloud) producing the σ bonds between the 1NNs. The majority spins are more equitably distributed (note the circular shape of the electron cloud) among the t_{2g} and e_g states. This is also consistent with the corresponding partial DOSs shown in Figs. 4(b) and 4(c), which we have discussed in the foregoing paragraph. The t_{2g} band is caused by the interatomic overlap between the $\{d_{xy}\}$ atomic orbitals of the 1NNs in the ⟨111⟩ directions while the e_g band is due to the $\{d_{z^2}\}$ atomic orbitals in the ⟨100⟩ directions. Consistent with the findings of Jones *et al.*,[50] the e_g states in bcc Fe increases the charge density on the cube surfaces (see the charge clouds along BB′C′C in Fig. 5). The overlaps of the e_g states may thus also contribute to the spin-spin coupling among both 1NN and 2NN, so that the exchange coupling between the 1NNs may have two contributions, one from the t_{2g} state and another from the e_g state.

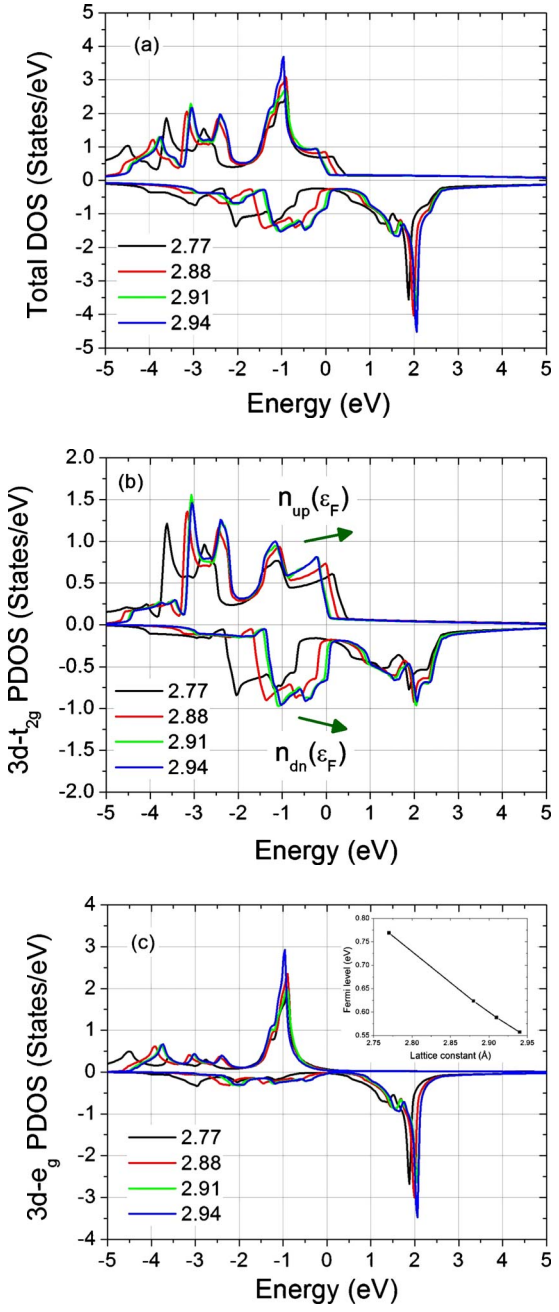

FIG. 4. (Color online) (a) Total and [(b) and (c)] partial 3*d*-DOS of bcc Fe for different lattice constants. The origin is set to its Fermi level for each lattice constant as shown in the inset of (c). The arrows show the change trend of DOS at Fermi level for spin up and spin down as decreasing the lattice constant.

As the interatomic separation increases, the electronic states become increasingly localized as the intersite overlap between the atomic orbitals decreases. It can be seen from Fig. 5 that the overlapping of the t_{2g} states between 1NNs decreases fast. It is practically cut off at a lattice constant of 2.94 Å, i.e., an interatomic separation of 2.55 Å. This decrease is consistent with the rapid narrowing of the t_{2g} band as the lattice constant increases in Figs. 3(c) and 4(b). Overlap of the e_g states, on the other hand, decreases more slowly, as can also be seen from the smaller change in the e_g band as

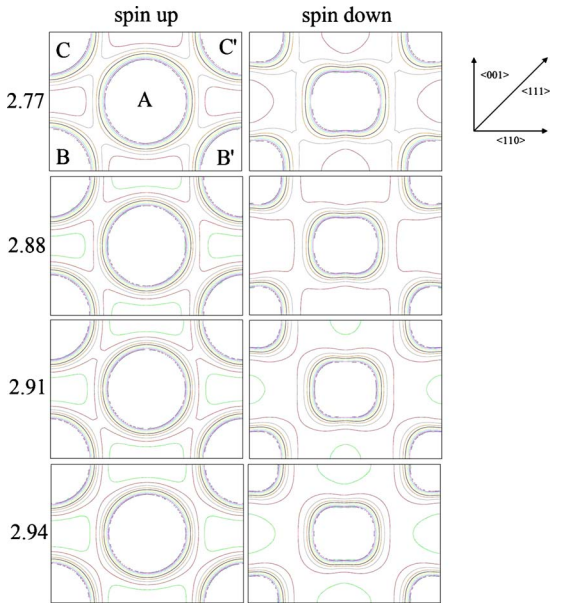

FIG. 5. (Color online) Charge-density map on (110) plane in bcc Fe with different lattice constants for both spin up and spin down with directions of the lattice vectors ⟨001⟩, ⟨111⟩, and ⟨110⟩ also shown.

shown in Figs. 3(d) and 4(c). Thus, the exchange coupling between the 1NNs may have a shorter-range contribution from the t_{2g} state which vanishes beyond ~2.55 Å, and a longer-range one from the e_g state. This also implies that the exchange coupling between the 2NNs may have contributions only from the e_g state.

As in Fig. 3, the spin densities, i.e., the number of electrons per atom N_l with orbital angular momentum l $(=s,p,d)$, can be calculated by integrating the corresponding partial DOS up to Fermi level, from which the corresponding local MMs $(\equiv N_l^{\uparrow} - N_l^{\downarrow})$ can also be obtained. The results are plotted as a function of the lattice constant in Fig. 6. In Fig. 6(a), the majority-spin density of *d* electrons increases from 3.7 to 4.6 per atom while the minority decreases from 2.4 to 1.9 as the lattice constant increases from 2.45 to 2.96 Å. We note that the total number of electron per atom on the *s*, *p*, and *d* orbitals is about 7. Approximately one electron is left in the interstitial region between the muffin-tin spheres because the muffin-tin spheres in WIEN2K only touch each other without overlapping and does not cover the entire region. The corresponding MM in Fig. 6(b) is an increasing function of the lattice constant, which practically accounts for all of the contributions to the MM in Fig. 2. That the MM is mainly due to the *d* orbitals and that the *s*, *p* contributions are negligible can also be seen directly from their respective spin densities in Fig. 6(b). The foregoing results are consistent with Frota-Pessoa *et al.*[50] who showed that the contributions to J_{ij}^{eff} is mainly due to the *d*-*d* interaction (+110%), contributions from the *p*-*d* interaction (−7%), and the *s*-*d* interaction are relative small.

Although it is generally accepted that GGA can give a better description of iron in many aspects,[36] it happens that the few calculations of J_{ij}^{eff} we found in the literature are all performed with LDA. To establish GGA for our calculations,

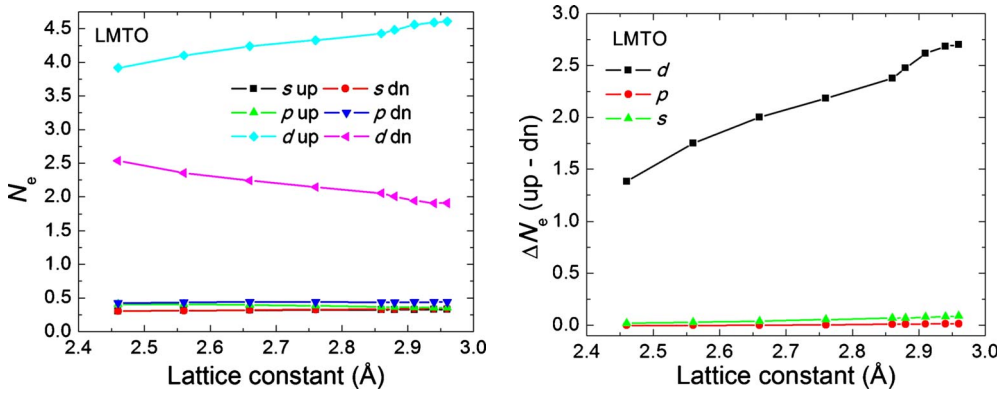

FIG. 6. (Color online) (a) The number of electrons on s, p, and d orbitals for spin-up and spin-down subbands, and (b) the corresponding magnetic moment component as a function of lattice constant. Here, data are obtained using LMTO-GF method.

we perform a comparison of the J_{ij}^{eff} obtained from both methods for the experimental equilibrium lattice constant (2.8665 Å). The results are listed in Table I. Our LDA results are in good agreement with those of other authors.[50–52] Except for the first two neighbor shells, J_{ij}^{eff} is smaller by at least an order of magnitude. In this regard, we note that the accuracy of the smaller components is very much limited by the tolerance set with the priority aim to maximize the efficiency of the calculation. The results reported in the following are obtained only using GGA.

In Fig. 7(a), we plot J_{ij}^{eff} as functions of the lattice constant from the 1NN to the ninth NN. For lattice constants smaller than 2.4 Å, the system is nonmagnetic with no MM and all components of J_{ij}^{eff} vanishes. It is obvious that J_1^{eff} and J_2^{eff} constitute the dominant contributions to the Heisenberg Hamiltonian. The LDA results obtained by Moran *et al.*[53] are shown for comparison. Despite the much larger values of their J_1^{eff} and J_2^{eff} compared with ours and those of Refs. 51–55, the slopes are similar. Unlike Moran *et al.*,[53] however, there is no cross over between J_1^{eff} and J_2^{eff} in our GGA results.

As discussed in the foregoing analysis based on DOS and the topological structure of the electronic distribution suggests that the exchange interactions between 1NNs atoms may have two contributions, one from the t_{2g} and the other from the e_g electrons, those between the 1NNs only have contributions only from the e_g electrons. If we speculate that the two-peak structure of J_1^{eff} is indicative of contributions, respectively, from the t_{2g} and e_g states, and the single-peak structure of J_2^{eff} suggests a single e_g contribution, we could explain very well the functional behavior of J_1^{eff} and J_2^{eff} in Fig. 7(a).

TABLE I. By using LMTO-GF, the value of J_{ij}^{e} (mRy) for bcc iron are calculated at the experimental lattice constant (2.8665 Å) as a function on the order of neighbor. Values from other works are also presented for comparison.

J_{ij}^{e} (mRy)	GGA	LDA	Ref. 50[a]	Ref. 51[b]	Ref. 52[c]
First	1.218	1.235	1.24	1.2	1.432
Second	1.080	0.799	0.646	0.646	0.815
Third	−0.042	−0.009	0.007	−0.030	−0.015
Fourth	−0.185	−0.128	−0.108	−0.100	−0.126
Fifth	−0.117	−0.093	−0.071	−0.068	−0.146
Sixth	0.061	0.044	0.035	0.042	0.062
Seventh	−0.013	0.001	0.002	−0.001	0.001
Eighth	0.017	0.018	0.014	0.014	0.015

[a]LDA; potential: not mentioned.
[b]LDA; potential: von Barth and Hedin.
[c]LDA; potential: Vosko-Wilk-Nusair.

Finally, we calculate the values of the most dominant components of the EIF, J_1 and J_2 from J_1^{eff} and J_2^{eff}, using the MM presented in Fig. 2 (LMTO-GF). The results are plotted as a function of the interatomic separation in Fig. 7(b). We note that the values of J_1 for an interatomic distance of less than 2.4 Å cannot be obtained this way, because the values of both J_1^{eff} and the MM vanish simultaneously in this range, where spin polarization disappears and the system is nonmagnetic.

The most prominent feature in Fig. 7(b) is the substantial difference between J_1 and J_2 for the same interatomic distance, highlighting the functional dependence on the atomic environment of J_{ij} as a function of the interatomic distance. Indeed, as inferred earlier from electron-structure considerations in relation to Figs. 3–5, J_1 has contributions from electron exchanges involving the overlaps of both t_{2g} and e_g states while J_2 only has contribution from the e_g overlap. The difference is attributed to the angular dependence of the electron charge distributions in a cubic lattice and is a many-body effect. In this regard, the relatively complex shape of J_1 could be the result of two superimposing Bethe-Slater-type curves corresponding to the respective singlet and triplet overlaps. Indeed, if we write $J_1=J_1^{t_{2g}}+J_1^{e_g}$ and $J_2=J_2^{e_g}$, and further assume that the e_g components of J_1 have the same shape that can be transformed from J_2 by simple rescaling according to $J_1^{e_g}=A_1J_2(\alpha_1 R)$, J_1 can be decomposed into its t_{2g} and e_g components by matching the corresponding peak position and peak height of the e_g component in J_1. Using $A_1=1.3$ and $\alpha_1=1.12$, we show in Fig. 7(c) that this simple interpretation can indeed give a very good representation of the relatively complex form of J_1. Indeed, in this representation, the t_{2g} component vanishes beyond a range of 2.55 Å, which is consistent with the electronic structure of the t_{2g} states, as discussed in the foregoing. We note that for negative values of J_{ij}, the magnetization vanishes and so does

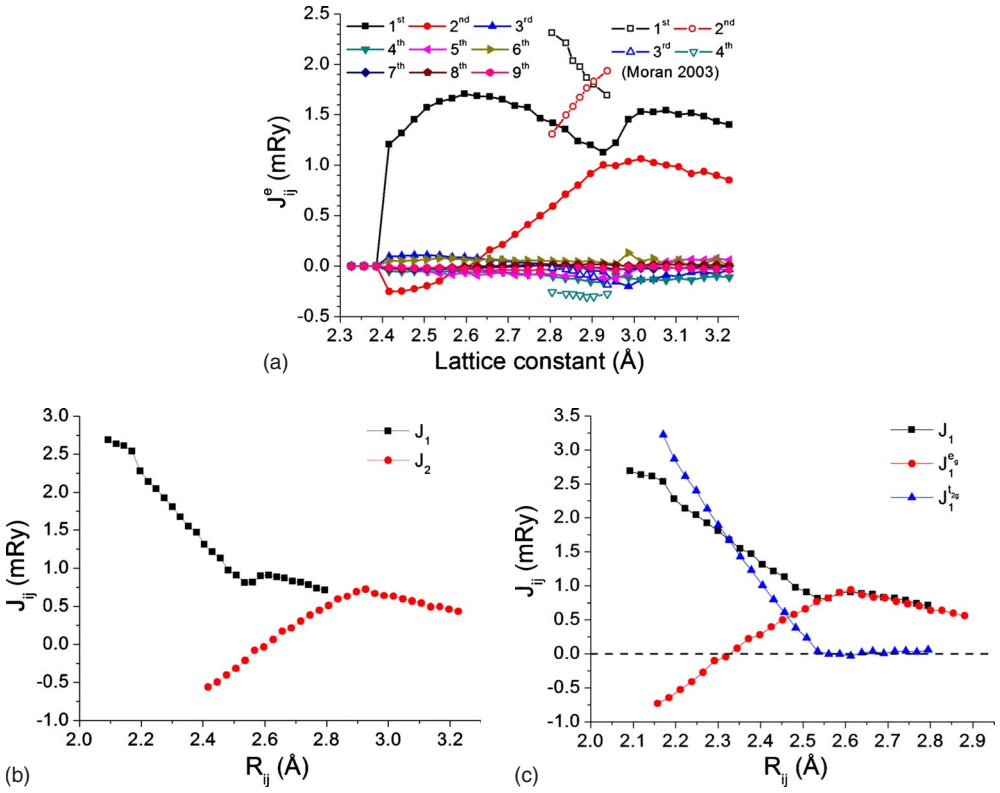

FIG. 7. (Color online) (a) The effective exchange interaction parameter J_{ij}^{e} from the first to the eighth neighbors as a function of the lattice constant a. Data from Morán *et al.* (Ref. 53) are also presented for comparison. (b) Components J_1 and J_2 plotted as a function of the interatomic distance with $R_1=\sqrt{3}a/2$ and $R_2=a$ being, respectively, the first- and second-nearest-neighbor distances. (c) Assuming a form for J_1: $J_1=J_1^{t_{2g}}+J_1^{e_g}$, where $J_1^{e_g}=A_1J_2(\alpha_1 R)$ with $A_1=1.3$ and $\alpha_1=1.12$, a very good representation of the relatively complex form of J_1 can be obtained.

J_{ij}^{eff}. Thus, only positive values of J_{ij} can be calculated from J_{ij}^{eff} and the negative values of $J_1^{t_{2g}}$ below ~2.1 Å can only be inferred.

IV. SUMMARY AND CONCLUSION

To perform large-scale dynamic atomistic simulation of magnetic materials, we need to consider the coupled dynamics of the spin and the lattice subsystems. Recent formulation of SLD allows the coupled dynamics to be modeled via the Heisenberg Hamiltonian. Explicit forms of the magnitude of the atomic spin polarization $S(\mathbf{R})$ and exchange interaction function $J_{ij}(\mathbf{R})$ are needed. In this regard, existent data useful for this purpose are only available in a restricted regime of small displacements from the equilibrium perfect lattice configurations. This strongly restricts the usefulness of SLD in simulations involving more general configurations. In this paper, *ab initio* calculations are performed to study the functional behavior of the exchange interaction function in bcc iron over a wide range of lattice constants using the magnetic force theorem and the one-electron Green's function. The associated electronic structure and atomic spin polarization are calculated using both LMTO-GF within ASA and WIEN2K based on the FP-LAPW method for comparison.

Our results suggest that $S(\mathbf{R})$ increases monotonically with the local atomic volume, starting from zero for an atomic volume corresponding to a lattice constant of ~0.23 nm. Physical arguments suggest that this functional behavior is due to effects that are many body in nature. We also found that $J_{ij}(\mathbf{R})$ has a rather complex functional form with strong dependence on the pair orientation derived from many-body effects, showing the inadequacy of the environment-independent pairwise functional representation assumed for convenience in previous works. Despite the relatively complex functional form from the data we obtained, we found that $J_{ij}(\mathbf{R})$ in bcc iron can be expressed as a superposition of Bethe-Slater curve representation of interatomic exchange integrals of the $3d$ electrons. Analyzing together with the associated electronic structure via the spin-split DOS and the electron density maps, the exchange interaction function between the 1NN could be explained by a sum of t_{2g} and e_g contributions, while that between the 2NN has a single origin from the e_g overlap.

ACKNOWLEDGMENTS

This project is initiated and funded by Grants No. 532008 and No. 534409 from the Hong Kong Research Grant Commission, to which the authors are thankful. The authors also would like to thank Derek A. Stewart for providing the LMTO-GF code (Ref. 29) and for useful discussions.

*Present address: EURATOM/CCFE Fusion Association, United Kingdom Atomic Energy Authority, Abingdon, Oxfordshire OX14 3DB, UK.
†Corresponding author; chung.woo@polyu.edu.hk

[1] H. C. Herper, E. Hoffmann, and P. Entel, Phys. Rev. B **60**, 3839 (1999).
[2] A. V. Ruban, P. A. Korzhavyi, and B. Johansson, Phys. Rev. B **77**, 094436 (2008).
[3] D. J. Dever, J. Appl. Phys. **43**, 3293 (1972).
[4] H. Hasegawa and D. G. Pettifor, Phys. Rev. Lett. **50**, 130 (1983).
[5] A. B. Sivak, V. A. Romanov, and V. M. Chernov, in *International Conference on Electron Microscopy and Multiscale Modeling*, edited by A. S. Avilov, S. L. Dudarev, and L. D. Marks (AIP, New York, 2007), pp. 118.
[6] M. L. Jenkins, Z. Yao, M. Hernández-Mayoral, and M. A. Kirk, J. Nucl. Mater. **389**, 197 (2009).
[7] S. Chiesa, P. M. Derlet, and S. L. Dudarev, Phys. Rev. B **79**, 214109 (2009).
[8] M. Y. Lavrentiev, D. Nguyen-Manh, and S. L. Dudarev, Phys. Rev. B **81**, 184202 (2010).
[9] G. Kresse and J. Furthmuller, Comput. Mater. Sci. **6**, 15 (1996).
[10] V. P. Antropov, M. I. Katsnelson, B. N. Harmon, M. van Schilfgaarde, and D. Kusnezov, Phys. Rev. B **54**, 1019 (1996).
[11] S. L. Dudarev and P. M. Derlet, J. Phys.: Condens. Matter **17**, 7097 (2005).
[12] S. L. Dudarev and P. M. Derlet, J. Phys.: Condens. Matter **19**, 239001 (2007).
[13] P. M. Derlet and S. L. Dudarev, Prog. Mater. Sci. **52**, 299 (2007).
[14] D. Nguyen-Manh, A. P. Horsfield, and S. L. Dudarev, Phys. Rev. B **73**, 020101 (2006).
[15] D. Nguyen-Manh, S. L. Dudarev, and A. P. Horsfield, J. Nucl. Mater. **367-370**, 257 (2007).
[16] P.-W. Ma, C. H. Woo, and S. L. Dudarev, Phys. Rev. B **78**, 024434 (2008); Philos. Mag. **89**, 2921 (2009).
[17] P.-W. Ma and C. H. Woo, Phys. Rev. E **79**, 046703 (2009).
[18] P. Mohn, *Magnetism in the Solid State* (Springer-Verlag, Berlin, 2003).
[19] L. Stixrude, R. E. Cohen, and D. J. Singh, Phys. Rev. B **50**, 6442 (1994).
[20] A. Dewaele, P. Loubeyre, F. Occelli, M. Mezouar, P. I. Dorogokupets, and M. Torrent, Phys. Rev. Lett. **97**, 215504 (2006).
[21] J. Kübler, *Theory of Itinerant Electron Magnetism* (Oxford University Press, New York, 2000).
[22] http://en.wikipedia.org/wiki/Exchange_interaction
[23] I. Turek, J. Kudrnovský, V. Drchals, and P. Bruno, Philos. Mag. **86**, 1713 (2006).
[24] F. Körmann, A. Dick, T. Hickel, and J. Neugebauer, Phys. Rev. B **79**, 184406 (2009).
[25] P. Blaha, K. Schwarz, G. K. H. Madsen, D. Kvasnicka, and J. Luitz, *WIEN2k: An Augmented Plane Wave+Local Orbitals Program for Calculating Crystal Properties*, edited by K. Schwarz (TU Vienna, Austria, 2009).
[26] O. Gunnarsson, O. Jepsen, and O. K. Anderson, Phys. Rev. B **27**, 7144 (1983).
[27] O. K. Andersen and O. Jepsen, Phys. Rev. Lett. **53**, 2571 (1984).
[28] M. van Schilfgaarde and V. P. Antropov, J. Appl. Phys. **85**, 4827 (1999).
[29] http://titus.phy.qub.ac.uk/Programs/LMTO/gf.html
[30] A. I. Liechtenstein, M. I. Katsnelson, and V. A. Gubanov, J. Phys. F: Met. Phys. **14**, L125 (1984).
[31] A. I. Liechtenstein, M. I. Katsnelson, and V. A. Gubanov, Solid State Commun. **54**, 327 (1985).
[32] A. I. Liechtenstein, M. I. Katsnelson, V. P. Antropov, and V. A. Gubanov, J. Magn. Magn. Mater. **67**, 65 (1987).
[33] J. P. Perdew, K. Burke, and M. Ernzerhof, Phys. Rev. Lett. **77**, 3865 (1996).
[34] J. P. Perdew and A. Zunger, Phys. Rev. B **23**, 5048 (1981).
[35] U. v. Barth and L. Hedin, J. Phys. C **5**, 1629 (1972).
[36] C. S. Wang, B. M. Klein, and H. Krakauer, Phys. Rev. Lett. **54**, 1852 (1985).
[37] M. Wuttig and X. Liu, *Ultrathin Metal Films: Magnetic and Structural Properties* (Springer-Verlag, Berlin, 2004).
[38] P. Bagno, O. Jepsen, and O. Gunnarsson, Phys. Rev. B **40**, 1997 (1989).
[39] R. Kohlhaas, P. Donner, and N. Schmitz-Pranghe, Z. Angew. Phys. **23**, 245 (1967).
[40] F. Birch, Phys. Rev. **71**, 809 (1947).
[41] M. Acet, H. Zähres, E. F. Wassermann, and W. Pepperhoff, Phys. Rev. B **49**, 6012 (1994).
[42] J. Łażewski, P. Piekarz, A. M. Oleś, and K. Parlinski, Phys. Rev. B **74**, 174304 (2006).
[43] Z.-Y. Zeng, C.-E. Hu, X.-R. Chen, L.-C. Cai, and F.-Q. Jing, J. Phys.: Condens. Matter **20**, 425217 (2008).
[44] C. Barreteau, M.-C. Desjonquères, A. M. Oleś, and D. Spanjaard, Phys. Rev. B **69**, 064432 (2004).
[45] P. Söderlind, R. Ahuja, O. Eriksson, J. M. Wills, and B. Johansson, Phys. Rev. B **50**, 5918 (1994).
[46] A. K. McMahan and R. C. Albers, Phys. Rev. Lett. **49**, 1198 (1982).
[47] V. Iota, J.-H. P. Klepeis, C.-S. Yoo, J. Lang, D. Haskel, and G. Srajer, Appl. Phys. Lett. **90**, 042505 (2007).
[48] M. Ekman, B. Sadigh, and K. Einarsdotter, Phys. Rev. B **58**, 5296 (1998).
[49] T. E. Jones, M. E. Eberhart, and D. P. Clougherty, Phys. Rev. Lett. **100**, 017208 (2008).
[50] S. Frota-Pessôa, R. B. Muniz, and J. Kudrnovský, Phys. Rev. B **62**, 5293 (2000).
[51] O. N. Mryasov, A. J. Freeman, and A. I. Liechtenstein, J. Appl. Phys. **79**, 4805 (1996).
[52] M. Pajda, J. Kudrnovský, I. Turek, V. Drchal, and P. Bruno, Phys. Rev. B **64**, 174402 (2001).
[53] S. Morán, C. Ederer, and M. Fähnle, Phys. Rev. B **67**, 012407 (2003).
[54] P. E. Blöchl, O. Jepsen, and O. K. Andersen, Phys. Rev. B **49**, 16223 (1994).
[55] J. M. Leger, C. Loriers-Susse, and B. Vodar, Phys. Rev. B **6**, 4250 (1972).